DOE-ET-53088-264 IFSR#264

KELVIN-HELMHOLTZ INSTABILITY AND VORTICES IN MAGNETIZED PLASMA

W. Horton, T. Tajima and *T. Kamimura**
Institute for Fusion Studies
The University of Texas at Austin
Austin, Texas 78712

* Institute for Plasma Physics, Nagoya, Japan

December 1986

Kelvin-Helmholtz Instability and Vortices in Magnetized Plasma

W. Horton and *T. Tajima*
Institute for Fusion Studies
The University of Texas at Austin
Austin, Texas 78712
and
T. Kamimura
Institute for Plasma Physics
of Nagoya University
Nagoya, Japan 464

Abstract

Analytic theory and implicit particle simulations are used to describe the evolution of the Kelvin-Helmholtz instability and the plasma vortices driven by a nonuniform $\mathbf{E} \times \mathbf{B}$ flow velocity. Formulas for plasma convection arising from the self-consistent plasma electric field give the rate of anomalous momentum transport across the magnetic field. The momentum transport is shown to be controlled by the tilting angle of the elliptical vortex with respect to the direction of the parallel flow. Three stages of evolution are investigated and formulas for the final vortex state are given.

I Introduction

There occur a number of situations in which an electric charge separation is set up across the magnetic field in a plasma. One example is the auroral oval region where hot magnetospheric ions are injected into colder ionospheric plasma, with hot ions causing charge separation.[1] Another example is an ignited plasma in the field reverse configuration (FRC) in which charged fusion products such as alpha particles or protons cause frictional transport of electrons in the radial direction.[2,3] The resulting crossed electric field $E_0(x)\hat{\mathbf{x}}$ and magnetic field $B_0\hat{\mathbf{z}}$ produces a sheared plasma $\mathbf{E}\times\mathbf{B}$ flow given by $v_y(x) = -cE_x/B_0$. When the strength of the sheared flow dv_y/dx exceeds a small critical value the plasma becomes unstable to the Kelvin-Helmholtz instability which feeds on the kinetic energy available in the relative streaming motion of the plasma. The maximum growth scales as $\gamma \sim \max|dv_y/dx|$ and occurs for wavelengths $\lambda_y \sim 4\pi a$ where a is the characteristic shear layer scale length $a^{-1} = \max|d\ln\ v_y/dx|$.

For strongly magnetized plasmas the Kelvin-Helmholtz growth rate is slow compared to the ion cyclotron frequency $|dv_E/dx| \ll \omega_{ci} = eB/m_ic$ and the wavelengths are long compared to the ion Larmor radius $a \gg \rho_i = v_i/\omega_{ci} = c(m_iT_i)^{1/2}/eB$. In this regime the use of traditional particle simulation methods would require a very large number of time steps and spatial cells to satisfy the conditions for stable pushing of Lorentz force driven particles. In contrast to the strongly charge separated case,[1] the large scale-slow instability hardly involves charge separation and is hydrodynamic in behavior. In addition, the plasmas of interest are sufficiently dense $\omega_{pi} \gg \omega_{ci}$ that the dynamics is determined by the condition of quasineutrality $\nabla\cdot\mathbf{j} = -\partial_t\rho_Q = 0$. To provide meaningful simulations in this situation a new simulation algorithm is used that follows the Lagrangian trajectories of guiding center particles retaining the inertial drifts. The algorithm uses implicit solutions for the electric fields and decentered particle dynamics with time steps $\Delta t\omega_{ci} \gg 1$ and space scales $\Delta x \gg \lambda_D$ for the Vlasov-Poisson system of equations. The technical aspects of the algorithm are given in Barnes et al.[4] In the work presented here we use the Barnes et al. algorithm for computations of the Kelvin-Helmholtz instability. For the theoretical analysis a simplified statement of the algorithm is used in the present work.

There are extensive earlier studies of a low density regime of the sheared flow instability as in Montgomery and Turner[5] and the references cited therein. In this regime $\omega_{pi} \ll \omega_{ci}$ the velocity of the plasma is computed neglecting the inertial acceleration. In the simplest

case only the $\mathbf{E} \times \mathbf{B}$ velocity is used to compute the particle motion and the Poisson equation is solved to obtain the electric field. In this so-called 2-D guiding center plasma the energy of the system is dominated by the electrostatic energy $\epsilon_{es} = (8\pi)^{-1} \int (\nabla\phi)^2 d^2x$ which is a constant of the motion since $\mathbf{j} \cdot \mathbf{E} \equiv 0$. In contrast in the K-H regime ($\omega_{pi} \gg \omega_{ci}$) the energy is dominated by the ion kinetic energy. Both regimes observe the nonlinear evolution by inverse cascade to large-scale vortex structures. In the low density guiding center plasma the nonlinear mode coupling is the $\mathbf{E} \times \mathbf{B}$ convection of the plasma density, while in the high density K-H regime the $\mathbf{E} \times \mathbf{B}$ convective derivative of the ion velocity is the nonlinear transfer mechanism.

In the guiding center plasma the density fluctuations are essential to the dynamics while in the high density regime the density fluctuations are relatively weak in the absence of a background density gradient. The work of Montgomery and Turner[5] considers the effect of the density fluctuations through the Gibbs ensemble calculation for their equilibrium spectral distribution $\left\langle |\delta n_{i,e}(\mathbf{k})|^2 \right\rangle$ in an isolated, dissipationless system.

The problem analyzed in this work is the nonlinear evolution of the Kelvin-Helmholtz (K-H) instability produced by applying a fixed external electric field $v_y(x) = -cE_{\text{ext}}(x)/B_0$ such that

$$v_y(x) = v_0 \tanh\left(\frac{x}{a}\right) \tag{1}$$

or its piece-wise linear approximation

$$v_y(x) = \begin{cases} v_0 & x \geq a \\ v_0 \dfrac{x}{a} & |x| \leq a \\ -v_0 & x \leq -a \end{cases} \tag{2}$$

The problem considered is that of a driven shear flow which arises in situations where the equilibrium plasma has nonambipolar losses that lead to the maintenance of background sheared flows. The nonambipolar background loses arise in nonaxisymmetric confinement systems and the edge plasma of tokamaks where the outer field lines are open to a sheath plasma at the limiter or divertor. In these and other situations the driven problem appears more relevant than the traditional initial value problem.

The total electric field is given by

$$E(\mathbf{x}, t) = -\nabla\Phi(\mathbf{x}, t) \tag{3}$$

where the electrostatic field arises from the nonequilibrium plasma motion given by

$$\nabla^2\Phi(\mathbf{x},t) = -4\pi\rho = -4\pi\sum_j e_j\delta\left(\mathbf{x}-\mathbf{r}_j(t)\right) - 4\pi\rho_{\rm ext}(x) \tag{4}$$

where the label j includes the initial data $\left(\mathbf{x}_{0j},\ v_{\|j}\right)$ for all particles, and the nonambipolar equilibrium field $E_{\rm ext}(x)$ satisfies $\partial_x E_{\rm ext} = 4\pi\rho_{\rm ext}(x)$.

To accommodate the quasilinearity of the dynamics for time scales $\Delta t\omega_{ci} \gg 1$, the charge density is computed by using an expansion[3] of $\mathbf{r}_j(t)$ which transforms Eq. (4) to

$$\nabla^2\Phi = -4\pi\sum_j e_j\delta\left(\mathbf{x}-\mathbf{R}_j(t)\right) - 4\pi\rho_{\rm ext}(x) \tag{5}$$

where the motion $\mathbf{R}_j(t)$ is that of the guiding centers given by

$$\frac{d\mathbf{R}_j}{dt} = \frac{c\mathbf{E}\times\mathbf{B}}{B^2} + v_{\|}\hat{\mathbf{b}} + \frac{c^2 m_j}{e_j B^2}\frac{d\mathbf{E}_\perp}{dt} \tag{6}$$

$$\frac{dv_{\|}}{dt} = \frac{e_j}{m_j}\hat{\mathbf{b}}\cdot\mathbf{E}. \tag{7}$$

From Eqs. (6) and (7) the plasma current from the guiding center motion is

$$\mathbf{j} = \sum_j e_j\frac{d\mathbf{R}_j}{dt}\delta\left(\mathbf{x}-\mathbf{R}_j(t)\right) \tag{8}$$

$$= \frac{c^2 m_i n_i(\mathbf{x},t)}{B^2}\frac{d\mathbf{E}_\perp}{dt} + \hat{\mathbf{b}}\sum_j\frac{n_j e_j^2}{m_j}\int_0^t E_{\|}dt'. \tag{9}$$

In the simulations the

$$\delta(\mathbf{x}-\mathbf{R}_j) \to h_a(\mathbf{x}-\mathbf{R}_j) \text{ where } h_a(\boldsymbol{\xi}) = (2\pi a_x a_y)^{-1}\exp\left(-\xi_x^2/a_x^2 - \xi_y^2/a_y^2\right)$$

is the particle form factor. The condition of quasineutrality follows from ∂_t of Eq. (5) and Eq. (8)

$$\nabla\cdot\mathbf{j} = \nabla\cdot\left(\frac{c^2 m_i n_i}{B^2}\frac{d\mathbf{E}_\perp}{dt}\right) + \nabla_{\|}j_{\|} = -\frac{\partial\rho_Q}{\partial t} \simeq 0. \tag{10}$$

The conservation of ions yields

$$\frac{\partial n_i}{\partial t} + \mathbf{v}_E\cdot\nabla n_i + \nabla\cdot n_i\mathbf{v}_p = 0 \tag{11}$$

where the term $\nabla\cdot n_i\mathbf{v}_p$ is of order ω/ω_{ci} compared with the leading terms. From Eqs. (10) and (11) if follows that the total $\mathbf{E}\times\mathbf{B}$ drift energy changes due to

$$\frac{d}{dt}\left[\frac{m_i}{2}\int n_i v_E^2 d\tau\right] = -\int j_{\|}E_{\|}d\tau. \tag{12}$$

For 2D motion $\varphi(x,y,t)$ in the uniform magnetic field $\mathbf{B} = B_0\hat{\mathbf{z}}$ the equations (10) and (11) reduce to

$$\nabla\cdot\left(n_i\nabla_\perp\frac{\partial\Phi}{\partial t}\right) + \frac{c}{B}\nabla\cdot(n_i[\Phi,\nabla\Phi]) = 0 \tag{13}$$

$$\frac{\partial n_i}{\partial t} + \frac{c}{B}[\Phi, n_i] = 0 \tag{14}$$

where the Poisson bracket $[f,g]$ is defined by

$$[f,g] = \hat{\mathbf{z}}\cdot\nabla f\times\nabla g = \frac{\partial f}{\partial x}\frac{\partial g}{\partial y} - \frac{\partial f}{\partial y}\frac{\partial g}{\partial x}. \tag{15}$$

For modes that are sufficiently constant along the magnetic field line that $\Phi(x,y,s) \simeq \langle\Phi\rangle$ where

$$\langle\bar{\Phi}\rangle = \int d\mathbf{v} f_e \frac{1}{\tau}\int\frac{ds}{v_\parallel}\Phi(x,y,s)$$

the 2-D approximation in Eqs. (13)–(15) follows from Eq. (10) by taking the $\int ds/B$ flux tube integral and using appropriate flux tube integrated plasma density in Eqs. (13)–(14). In contrast, when the potential drops by $\Delta\Phi \sim \Phi$ over a distance ΔL along the field line the $\nabla_\parallel j_\parallel$ in Eq. (10) must be computed from the bounce averaged electron kinetic equation. The divergence of the parallel electron current brings in the coupling of the K-H mode to the electron drift wave through

$$\nabla_\parallel j_\parallel = \frac{e^2 N_e}{T_e}\left[\frac{\partial}{\partial t} + (\mathbf{v}_E + \mathbf{v}_{de})\cdot\nabla\right]\left(\Phi - \left\langle\bar{\Phi}\right\rangle\right)$$

where $\mathbf{v}_{de} = -(cT_e/eB)\,\hat{\mathbf{z}}\times\nabla\ln N_e$.

In the limiting case where the background plasma density is constant $\nabla\ell n\, N_e \simeq 0$ the density fluctuations $\tilde{n}_k = (\omega - k_y v_0)^{-1}\mathbf{k}\cdot\mathbf{v}_{k_1}\tilde{n}_{k_2}$ from Eq. (14) are second order, and the dynamics (13)–(14) reduces to that of the 2D convective cells identical to the 2D incompressible Euler flow[7] with stream function $\varphi = c\Phi/B$. The 2D equations for vorticity ζ are

$$\partial_t\zeta + [\varphi,\zeta] = 0 \tag{16}$$

$$\nabla^2\varphi = \zeta. \tag{17}$$

In the simulations investigated here the background density is taken as constant so that Eqs. (16) and (17) describe the $\omega_{pi} \gg \omega_{ci}$ dynamics for the 2D simulations with $\mathbf{B} = B_0\hat{\mathbf{z}}$. The density fluctuations are observed to satisfy the condition $\tilde{n} < n_0\tilde{v}/v_0$.

The stream function $\varphi = c\Phi/B$ has units of diffusivity and scales as $D_B = ck_BT_e/eB$ for potentials $e\Phi \simeq k_BT_e$ controlled by the electron temperature.

In the regime where the magnetic field is tilted in the y-direction such that $E_{\|} = B_yE_y/B_0 = -(B_y/B_0)\partial\Phi/\partial y$ is appreciable the dynamics becomes of the drift wave type once $k_yv_e|B_y/B_0| > |\omega|$. In this regime the parallel divergence does not vanish and is given by

$$\nabla_{\|}j_{\|} = e\frac{\partial n_e}{\partial t} \simeq \frac{e^2N_e}{T_e}\frac{\partial\Phi}{\partial t}. \tag{18}$$

Substituting Eq. (18) into Eq. (10) yields the shielded convective cell equation

$$\left(1 - \rho_s^2\nabla_{\perp}^2\right)\frac{\partial\varphi}{\partial t} - \left[\varphi, \rho_s^2\nabla^2\varphi\right] = 0 \tag{19}$$

where $\rho_s = c(m_iT_e)^{1/2}/eB$. Equation (19) describes the Kelvin-Helmholtz instability as modified by the finite $E_{\|}$ and the associated parallel electron current $j_{\|}$.

In the presence of $\nabla_{\|}j_{\|}$ given by Eq. (18) the power balance Eq. (12) yields the energy integral

$$E = \frac{m_i}{2}\int n_iv_E^2d\tau + \frac{e^2}{2T_e}\int N_e\Phi^2d\tau.$$

Both the 2D flute or convective cell dynamics (16)-(17) and the 2D drift wave dynamics (19) have enstrophy integrals U_1 and U_2, respectively. For (16)-(17)

$$U_1 = \frac{1}{2}\int\zeta^2d\tau = \frac{1}{2}\int(\nabla^2\varphi)^2d\tau = \text{const.}$$

and for (19)

$$U_2 = \frac{1}{2}\int\left[(\nabla\varphi)^2 + (\nabla^2\varphi)^2\right]d\tau = \text{const.}$$

In addition, both systems conserve the total momentum $P_y = m_i\int n_iv_yd\tau$ when the external force $F_y = -\langle j_x\rangle B_z/c$ vanishes at the x-boundaries.

II Simulation Experiments and Linear Instability

The 2D simulations are performed in a box of width L_x and length L_y parallel to the reversed flow $v_y(x)$. The system is periodic in y and has conducting wall boundaries at $x = 0$ and $x = L_x$ with $v_x(0) = v_x(L_x) = 0$. The Lorentz force equations are made dimensionless by introducing the variable space scale Δ_x (in the x-direction) and time scale ω_{pe}^{-1}; that is $x = \Delta_x\hat{x}$, $t\omega_{pe} = \hat{t}$. The units of the electric and magnetic fields are $E = \left(m_e\Delta_x\omega_{pe}^2/e\right)\hat{E}$ and $B = (m_ec\omega_{pe}/e)\hat{B}$ or $\hat{B} = \omega_{ce}/\omega_{pe}$. The dimensionless $\mathbf{E}\times\mathbf{B}$

velocity is $\hat{v} = v_E/\Delta_x\omega_{pe} = \hat{E}/\hat{B}$. In the reference case the simulation parameters are $a = 10\Delta_x$, $\omega_{pe}\Delta t = 200$, $L_x/\Delta_x = L_y/\Delta_y = 64$ and the number of particles per cell $N_e = N_i = 9$ per cell. The mesh size in the y-direction is either $\Delta_y/\Delta_x = 1$ or 2. The particles are taken as gaussian clouds with size $a_x = 3\Delta_x$ and $a_y = 3\Delta_y$. The time decentering parameters of the Lorentz force are $\alpha_i = \alpha_e = 0.1$.

The space time scales $(\Delta_x, \omega_{pe}\Delta t)$ in this new algorithm may be chosen to represent the space-time scales that dominate the physical problem of interest, in contrast to the conventional explicit particle simulation code in which the scales are fixed by $\Delta \cong \lambda_{De}$ (the Debye length) and $\omega_{pe}\Delta t < 1$ We wish to study the low frequency $\omega \sim v_0/a \ll \omega_{ci}$ regime of the Kelvin-Helmholtz instability for realistic ion-to-electron mass ratios, where a is the velocity shear gradient length. Thus, we take $m_i/m_e = 1600$ and the magnetic field strength $\omega_{ce}/\omega_{pe} = 10 - 80$. The space scales L and Δ_x are to range over the longest to shortest wavelength of interest which requires $L > a \gg \Delta_x$.

The time step is determined by $v_{\max}\Delta t < \Delta \equiv \min(\Delta_x, \Delta_y)$ the Courant condition. We limit the maximum flow velocities to be such that the maximum frequency $v_{\max}/\Delta$ in the dynamics is $\omega_{\max} = \pi v_{\max}/\Delta \ll \omega_{ci}$. The fastest large space scale dynamics is then on the frequency $\omega_k \sim kv_{\max} = 2\pi m v_{\max}/L = m\omega_{ci}(2\pi\Delta/10L) \sim m\omega_{ci}/100$.

The reference time step is then $\Delta t v_{\max} < \Delta$ or $\Delta t\omega_{pe} = \Delta\omega_{pe}/v_{\max} = 10\omega_{pe}/\omega_{ci} = 200$. In the problem with $B_y/B_0 = 0$ or $k_{||} = 0$ the distribution of particles in $v_{||}$ has no effect on the dynamics of the instability. Here, we consider primarily this regime with $k_{||} = k_y B_y/B_0 = 0$.

A Simulation Experiments

A nonuniform time series at eight times $\omega_{ci}t_n$ $n = 1, 2, \ldots 8$ are shown for Expt. 1 in Figs. 1-2. The initial flow in Eq. (1) is perturbed by a small amplitude (1%) $m = 3$ perturbation in the initial x position $x = x_0 + \delta\cos(k_s y)$. After a transient the exponential growth of the unstable mode dominates in frames (b)–(c) of Fig. 1 giving the contours of the electrostatic potential $\varphi(x, y, t)$.

In Fig. 2 we show the particle motion in the x-y plane perpendicular to the magnetic field. In Fig. 2 only those particles with initial velocities $v_y < 0$, i.e. those to the left of the $v_y = 0$ symmetry line, are plotted. From Fig. 2 we first see tongues of particles moving across the symmetry line from $v_x = cE_y/B$. Subsequently, these tongues undergo

$\mathbf{E} \times \mathbf{B}$ trapping into vortical motions in the x-y-plane. The dominant velocity of both the ions and electrons is from the $\mathbf{E} \times \mathbf{B}$ drift which is the same for both species and is a $1\frac{1}{2}D$ Hamiltonian flow $\dot{x} = -\partial_y \varphi(x,y,t)$, $\dot{y} = \partial_x \varphi(x,y,t)$ produced by the plasma potential $\varphi(x,y,t) = c\Phi_k/B$. The $\mathbf{E} \times \mathbf{B}$ trapping of the guiding center particles occurs in the region around $v_y = 0$ given by $v_0 x^2/2a \leq c\varphi_k(x=0)/B$ growing exponentially $x_T/a = [c\varphi_k(t)/\mathrm{Bav}_0]^{1/2}$ in time.

Comparing the particle phase space in Fig. 2 with the potential contours in Fig. 1 shows the typical phenomena that the particle orbits become strongly stochastic while the potential $\varphi(x,y,t)$ is relatively smooth and slowly varying. This stochasticity phenomena is shown to be generic for $\mathbf{E} \times \mathbf{B}$ motion in low frequency waves by Horton.[8] Qualitatively, the stochasticity sets in for small perturbations from the integrable single wave system due to the sensitivity of the stagnating (or separatrix) flows that occur between the regions of convection created by the local maxima and minima of the $\varphi(x,y)$ potential.

The electrostatic potential obtained from the inversion in Eq. (5) strongly smooths the irregularities of the stochastic charge density. Initially the most important role of the stochasticity is to break the symmetry of the regular chain of linear vortical flows. With the symmetry broken the neighboring regions of like vorticity begin the merging process characteristic of 2D hydrodynamics. In Figs. 1 c-d we see the merging of the three vortices or islands of excess negative vorticity $\zeta = \nabla^2 \varphi$ into two islands. In Figs. 1d-f we see the merging from two to one large vortex. This phenomena of like vortex merging is well known in 2D fluid dynamics, and is probably the dominant nonlinear process taking the plasma to the quasi-stationary final state. The final state (in these computations) is a large vortex of the size of the simulation box. The final vortex appears to maintain a certain degree of spatial and temporal irregularity or chaos for long time. From the particle phase space the irregularity would appear to be maintained by the continued global stochasticity in the Lagrangian trajectories.

The merging of the small islands or vortices to form large vortices is a manifestation of mode coupling $\sum \mathbf{k} \times \mathbf{k}_1 \cdot \hat{\mathbf{z}}(k_2^2 - k_1^2)\varphi_{k_1}\varphi_{k_2}$ in Eq. (14) to transfer energy from large k to small k. In regimes of large L/a the irregularities of the flow become sufficient that statistical turbulent approximations for $\varphi(x,y,t)$ may become very roughly applicable. In the description of turbulence theory the build-up of large scale vortices is the inverse cascade process in which energy is transferred from high k to low k. In terms of renormalized turbulence theory the rate of the build of low-k energy is given by a negative eddy or

turbulent viscosity $\nu_{k<k_c}$ from mode coupling which transfers energy from large k modes to small k modes in the spectral equation for $E(k,t)$. In the regimes with large L/a the irregularities of the flow are sufficient that the turbulent approximation of an inverse cascade may begin to apply. In this regime renormalized turbulence theory predicts a k dependent eddy viscosity ν_k which is driven up when the high k part of the fluctuation spectrum is sufficiently strong. It appears unlikely that the $\varphi(x,y,t)$ fields generated in the present simulations are sufficiently chaotic to allow the turbulence theory calculations to give more than a qualitative description of the dynamics.

B Linear Eigenmodes

The early evolution of the system from profile (1) or (2) is investigated using the linear dynamics of the hydrodynamic model given in Eq. (16). We write the potential as

$$\varphi(x,y,t) = \varphi_0(x) + \sum_{k_y>0} \left[\varphi_{k_y}(x,t)e^{ik_y y} + \varphi^*_{k_y}(x,t)e^{-ik_y y}\right] \tag{20}$$

with $k_y = 2\pi m/L_y$. The linear eigenmodes of Eqs. (16)-(17) $\varphi_k(x,t) = \varphi_k(x)\exp(-i\omega t)$ satisfy

$$\frac{d^2\varphi_k}{dx^2} - k^2\varphi_k - \frac{kv_0''(x)}{kv_0(x)-\omega}\varphi_k(x) = 0 \tag{21}$$

where $v_0'' = d\zeta/dx$ is the gradient of the vorticity. For the hyperbolic tangent profile in Eq. (1) only the marginally stable points $k_y a = 0$ and $k_y a = 1$ where $\omega = 0$ can be found analytically. For the piece-wise continuous profile in (2) the analytic solution[9] is straightforward, and we use that solution in the following analysis with the understanding that the abrupt changes at $x = \pm a$ are idealizations for continuous $v_y(x)$ profiles.

The dispersion relation for profile (2) is shown in Fig. 3 and has purely growing modes for $ka < k_c = 0.628$

$$\omega_k = \pm i\gamma_k = \pm\frac{v_0}{2a}\left[e^{-4ka} - (1-2ka)^2\right]^{1/2} \tag{22}$$

and two running waves for $ka > k_c$

$$\omega_k = \pm\frac{v_0}{2a}\left[(1-2ka)^2 - e^{-4ka}\right]^{1/2}. \tag{23}$$

The growth rate γ_k is a maximum at $k_m a = 0.377$ where $\gamma_m = 0.20(v_0/a)$ compared with corresponding values of 0.45 and 0.190 for the hyperbolic tangent profile in Eq. (1).

The wave functions $\varphi_k(x)$ for the unstable spectrum are symmetric in amplitude $\varphi_k(x)$ about $x = 0$ and have an antisymmetric phase shift $\theta_k(x) = \arg[\varphi_k(x)]$. The amplitude and

phase are shown in Fig. 4. A simple special case occurs for $k_y a = 1/2$ where $\gamma_k = v_0 e^{-1/2}/2a$ and

$$\varphi_k(x) = A_k \left[\cosh\left(\frac{x}{2a}\right) + i \sinh\left(\frac{x}{2a}\right) \right]. \tag{24}$$

For this mode the amplitude is $A_k \left[2\cosh^2\left(\frac{x}{2a}\right) - 1 \right]^{1/2}$ and the phase shift $\theta_k(x) = \tan^{-1}\left[\tanh(x/2a)\right]$. The $\mathbf{E} \times \mathbf{B}$ flow given by an unstable mode is shown in Fig. 5. The phase shift $\theta_k(x)$ displaces the two chains of linear vortices by approximately one half wavelength. The result of the phase shift is to make a net flow across the sheared layer that alternately takes $v_y > 0$ plasma to the left by $v_x < 0$ and $v_y < 0$ plasma to the right by $v_x > 0$ convection. The net convective momentum flux $\pi(x,t)$ is computed in the following section and shown in Fig. 4b.

The necessary condition for unstable roots of Eq. (20) is the Rayleigh condition that the gradient of the vorticity $\zeta' = v_0''(x) = 0$ for $x = x_m$ in the profile. The marginally stable mode has $\omega = k_y v_0(x_m)$. For antisymmetric profiles $v_0(x)$ the onset occurs where $\omega_m = k_y v_0(x_m) = 0$. Since the last mode to be stabilized as the profiles $\{v_0(x)\}$ relax is the $k_y \to 0$ mode, a sufficient condition[10] for instability follows from the $k_y = 0$ solution of Eq. (21). For rigid, conducting walls at $x = \pm L/2$ the dispersion relation for

$$c = \lim_{k_y \to 0} \left(\frac{\omega}{k_y} \right) \tag{25}$$

is

$$D(c, L/a) = \int_{-L/2}^{L/2} \frac{dx}{\left[c - v_0(x/a)\right]^2} = 0 \tag{26}$$

with analytic continuation from $\mathrm{Im}(c) > 0$. For the piece-wise linear profile $D(c, L/a) = (L - 2a)(c^2 + v_0^2)/(c^2 - v_0^2)^2 + 2a/(c^2 - v_0^2)$ showing the beam-plasma character of the $k_y a \to 0$ modes. The condition for instability is $L > 4a$ for the piece-wise linear profile. For the hyperbolic tangent profile (1), the sufficient condition for unstable eigenmodes is $L > 2.4a$ derived from the $D(c = 0, L/a) = 0$ condition.

C Anomalous Momentum Flux and Energy Transfer

The net x-flux of y-momentum per unit mass across a constant x surface is given by

$$\pi(x,t) = \langle v_x v_y \rangle = \sum_{k_y > 0} i k_y \left(\varphi_k^* \frac{d\varphi_k}{dx} - \varphi_k \frac{d\varphi_k^*}{dx} \right). \tag{27}$$

The net flux of vorticity $\zeta = \nabla^2\varphi$ across the x-surface is given by

$$\langle v_x\zeta\rangle = \sum_{k_y>0} ik_y\varphi_k^*\zeta_k = \frac{d\pi(x,t)}{dx}. \tag{28}$$

The non-vanishing momentum flux arises from the phase shift and is shown in Fig. 4b. Introducing the amplitude and phase into Eq. (27) yields

$$\pi(x,t) = -\sum_{k_y} k_y \frac{d\theta_k}{dx} |\varphi_k(x,t)|^2 . \tag{29}$$

For the eigenfunctions of profile (2) shown in Fig. (4) the flux reduces to

$$\pi(x,t) = -\sum_{k_y} k_y^2 |\varphi_k|^2 \quad \text{for} \quad |x| \le a, \tag{30}$$

and $\pi(x,t) = 0$ for $|x| > a$. The calculation of the total flow $\varphi(x,y,t)$ from the linear eigenfunction for $m = 1$ and the corresponding flux π is shown in Fig. 6.

The tilting of the vortices arises from the phase shift as modeled by the form

$$\varphi = \varphi_0 + A_k(x,t)\cos\left[k_y(y+\alpha x)\right]. \tag{31}$$

It is easy to see from Fig. 7 or from Eqs. (27) and (31) that the momentum flux is proportional to the angle α of the tilting,

$$\pi_k = -\frac{k^2 A_k^2(x)}{4}\alpha.$$

The momentum flux π reduces the strength of the initial sheared flow profile $v_y(x)$. The evaluation of the y-average $\langle\ \rangle = \int d_y/L_y$ vorticity and velocity profile are given by

$$\frac{\partial\zeta(x,t)}{\partial t} + \frac{\partial}{\partial x}\langle v_x\zeta\rangle = 0 \tag{32}$$

and

$$\frac{\partial v_y(x,t)}{\partial t} + \frac{\partial}{\partial x}\pi(x,t) = 0. \tag{33}$$

The flux of vorticity equals the gradient of the momentum flux, $\langle v_x\zeta\rangle = \partial\pi/\partial x$, and is the effective tangential drag force acting between the counter flowing streams. The drag in Eq. (33) arises from the convection of the flow across the shear layer due to either the Kelvin-Helmholtz fluctuations or vortices.

It is straightforward to show that the transfer of kinetic energy from the mean flow $v_y(x,t)$ to the fluctuating flow is given by $v_y(\partial\pi/\partial x)$, which in general is positive definite. The energy conservation theorem is obtained by defining

$$T = \frac{1}{2}\int_{x_1}^{x_2} v_y^2(x,t)dx, \qquad E = \frac{1}{2}\int \left\langle \left(\tilde{v}_x^2 + \tilde{v}_y^2\right)\right\rangle dx \tag{34}$$

and showing that

$$\frac{dT}{dt} = -\int_{x_1}^{x_2} v_y \frac{\partial \pi}{\partial x} dx \tag{35}$$

$$\frac{dE}{dt} = \int_{x_1}^{x_2} v_y \frac{\partial \pi}{\partial x} dx - F_E(x,t) \Big|_{x_1}^{x_2}, \tag{36}$$

where $\int dx v_y \partial \pi / \partial x$ is a three point correlation function of the φ-field and $F_E = \frac{1}{2} \langle \tilde{v}_x \tilde{\mathbf{v}}^2 \rangle$ is the flux of fluctuation kinetic energy.

The transport described by the quasilinear approximation appears to be the dominant process, as evidenced by the linear chain of titled vortices, until the strength of the convection reaches the strong mixing level given by

$$\mathbf{k} \cdot \mathbf{v}_E = \frac{c k_x k_y}{B} \tilde{\varphi} > k_y v_0. \tag{37}$$

At this level the flow is strongly nonlinear with $[\varphi, \nabla^2 \varphi] > \nabla^2 \partial_t \varphi$ in the bulk of the vortex. Here we look for exact stationary nonlinear solutions for the vortical flow. The mixing length level given by Eq. (37) may also be expressed as $\tilde{\varphi} = k_x^{-1} |d\Phi/dx|$ where $d\Phi/dx$ is the potential gradient across the sheared layer of width a. Since $k_x^{-1} = k_y^{-1} \sim 2a$, condition (37) gives the fluctuating potential $\tilde{\varphi}$ is of the order of the equilibrium potential difference $\Delta\Phi$ driving the sheared flow.

Now we consider the effect of viscosity on the stability of the modes. The viscosity may arise from ion-ion collisions or as a model for the effect of the high $\mathbf{k}$ mode coupling as an eddy damping mechanism.

D Effects of Dissipation

In the dissipationless limit the short wavelength modes $k_y a > k_c$ are marginally stable, beam-like modes with $\omega_k = \pm(k_y v_0 - v_0/2a)$. The eigenfunctions are exponentially localized to within $1/k_y$ of the velocity surfaces $\omega/k_y = \pm v_0$ where the vorticity gradient $\zeta' = v_0''(x)$ is maximum. These localized modes are sensitive to ion-ion collisional or turbulent eddy damping viscosity effects due to their sharp spatial gradients. We derive the new transcendental dispersion relation containing the effect of the viscosity force $\nu \nabla^2 \mathbf{v}$ on the sheared flow.

Including a weak viscosity force $\nu \nabla^2 \mathbf{v}$ in the ion momentum balance equation adds the diffusion term $\nu \nabla^2 \zeta$ to the right-hand side of the vorticity Eq. (16). The linear eigenmodes of Eqs. (16) and (17) are now given by

$$\left[\omega - k_y v_0(x) - i\nu \left(\partial_x^2 - k_y^2\right)\right] \left(\partial_x^2 - k_y^2\right) \varphi_k(x) + k_y v_0''(x) \varphi_k(x) = 0 \tag{38}$$

which is called the Orr-Sommerfeld equation. For the piecewise continuous profile (2) where $v_0''(x) = (v_0/a^2)[\delta(x+a) - \delta(x-a)]$ the WKB solutions of Eq. (38) are

$$\varphi_k^{(\alpha)} = \sum_{\pm} A_{\pm}^{(\alpha)} e^{\pm k_y x} + B_{\pm}^{(\alpha)} e^{\pm \int_0^x \left(k_y^2 + K^2(x')\right)^{1/2} dx'}$$

where

$$K^2(x) = \frac{-i}{\nu}[\omega - k_y v_0(x)]$$

and $\alpha = 1, 2, 3$ for the three regions $x = [-L/2, -a, a, L/2]$. The dispersion relation follows from requiring continuity of φ_k, φ_k', φ_k'' at $x = \pm a$ and matching the jump in φ_k''' with the jump in v_0' at $x = \pm a$. We define

$$\beta_k(\omega) = \int_{-a}^{a} dx' \left[k_y^2 + K^2(x')\right]^{1/2} = -\frac{2i\nu a}{3k_y v_0}\left[\left(k_y^2 + K_+^2(\omega)\right)^{3/2} - \left(k_y^2 + K_-^2(\omega)\right)^{3/2}\right]$$

where

$$K_{\pm}^2 = -\frac{i}{\nu}(\omega \mp k_y v_0) \tag{39}$$

and obtain the dispersion relation

$$D\left(\frac{\omega a}{v_0}, k_y a, \frac{\nu}{v_0 a}\right) \tag{40}$$

$$= \left[\omega - k_y v_0 + \frac{v_0}{2a}\left(1 - \frac{k_y}{\left(k_y^2 + K_+^2\right)^{1/2}}\right)\right]\left[\omega + k_y v_0 - \frac{v_0}{2a}\left(1 - \frac{k_y}{\left(k_y^2 + K_-^2\right)^{1/2}}\right)\right]$$

$$+ \frac{v_0^2}{4a^2}\left[e^{-2k_y a} - \frac{k_y e^{-\beta_k(\omega)}}{\left(k_y^2 + K_+^2\right)^{1/2}}\right]\left[e^{-2k_y a} - \frac{k_y e^{-\beta_k(\omega)}}{\left(k_y^2 + K_-^2\right)^{1/2}}\right] = 0. \tag{41}$$

The $D(\hat{k}, \hat{\omega}, \hat{v}) = 0$ dispersion relation is a transcendental function with an infinite number of roots. The effect of finite ν on the K-H mode is to reduce the critical wavenumber $k_c(\nu)$ and to shift the maximum growth rate to lower $k_m(\nu)$. The magnitude of the maximum growth rate is only weakly changed by ν as shown in Fig. 8. Above $k_c(\nu)$ the K-H mode is weakly damped with $\hat{\omega} \cong \hat{k} - 1/2 + \hat{k}\hat{\nu}^{1/2}(1-i)/2$. A new beam-like mode appears with $\omega \simeq k\left[1 - i0.5\hat{\nu}\exp(-4\hat{k})\right]$ (not shown in Fig. 8). This mode is localized to the steps in vorticity at $x = \pm a$ and may not be accurately represented in this simple analytic model.

In addition to the eigenmodes given by $D(\omega, k, \nu) = 0$ there are transient or ballistic modes that propagate with the local fluid velocity $\omega = k_y v_0(x) - ik_\perp^2 \nu$. For smooth initial perturbations with many modes these transients phase mix away. The decay time may be long, however, at the critical points $v(x) = \pm v_0$ where there is a neighboring beam-like

eigenmode and at $v_0(x) = 0$ where for finite amplitude there is immediate trapping and mixing of the counter-streaming flows.

The ballistic modes follow from retaining the initial value term $\varphi_k(x, t = 0)$ in the solution of Eq. (14) which leads to the approximate solution for the transit response

$$\varphi_{k_y}(x,t) = \int_{-\infty}^{+\infty} \frac{G_{k_y}(x,x')\varphi_k(x',t=0)e^{ik_y(y-v_0(x')t)-\int_0^t \nu k_\perp^2 dt'}}{D_{k_y}(\omega = k_y v_0(x') - ik_\perp^2\nu)}dx'. \tag{42}$$

At early times $k_y \Delta v_0 t \ll 1$ the initial perturbation propagates as $\varphi(x, y, t) = \varphi(x, y - v_0(x)t, 0)$. The effective value of ν thus increases secularly as $\nu\nabla^2\zeta_k = -\nu k_y^2(1 + v_0'^2 t^2)\zeta_k$ due to the sheared flow. For times greater than $k_y v_0' \Delta x t > 1$ where Δx is the width of the initial perturbation the disturbance phase mixes away. The exact expression for the Green's function $G_{k_y}(x, x')$ is too complicated to present in detail.

For $k_y a > k_c = 0.628$ the eigenmodes are right and left running waves increasing from zero speed to $\pm v_0\,(1 - 1/2k_y a)$ as shown in Fig. 3. Thus, in the solution of the initial value problem there is a double root of the response function for ballistic modes in the shear layer. The double root starts at $x = 0$ for $k_y a = k_c$ and increases to $(x/a)_r = \pm\,(1 - 1/2k_y a)$ for $k_y a \gtrsim k_c$. For initial condition with nonvanishing vorticity in the shear layer, the resonant ballistic response grows as $t \exp\,[-ik_y v_0(x_r)t]$. These secularly growing resonant modes are observed in the simulation when L_y is chosen such that all the $k_y = 2\pi m/L_y$ modes $(m \neq 0)$ are above k_c.

The effect of an electron friction force $-\nu_e \mathbf{v}_e$ from either electron-neutral collisions, or a model for electron-ion collisions, has also been analyzed. The resulting stability equation is

$$\left(\omega - k_y v_0(x) + i\frac{\chi}{1+\chi}\frac{\nu_e \omega_{ci}}{\omega_{ce}}\right)\left(\partial_x^2 - k_y^2\right)\varphi_k(x) + k_y \frac{d^2 v_0}{dx^2}\varphi_k(x) = 0. \tag{43}$$

In this calculation the result of keeping a finite $\chi = \omega_{pi}^2/\omega_{ci}^2$ cross-field susceptibility is also retained. We see that the dispersion relation is the same as given in Eq. (20) with the replacement $\omega_{k_y} \rightarrow \omega_{k_y} - i(m_e\nu_e/m_i)[\chi/(1+\chi)]$. The effect of the electron friction is a weak damping that gives rise to a low $k_y v_0$ threshold, $k_y|v_0| > 2m_e\nu_e/m_i$, for instability. Stabilization from the resistive dissipation of parallel currents $\eta j_{||} = E_{||}$ obtained by adding $\nabla_{||} j_{||} = -\nabla_{||}^2\varphi/\eta$ to Eqs. (10) and (12) is investigated by Chiueh[11] et al. The stabilization is weak at small $k_{||}$ or small magnetic shear $k_{||} = k_y x/L_s$.

E Nonlinear Stability

At the end of the exponential growth given by Eq. (37) where $\tilde{v}_y \simeq v_0$ the system evolves slowly as a vortex chain of finite amplitude and well-defined periodicity k close to that of the fastest growing initial mode. A reasonable nonlinear model of the observed vortex chain is given by the exact vortex chain solution of Eqs. (16) and (17)

$$\varphi(x,y) = \frac{v_0}{k}\ell n\left[\cosh(kx) - \phi_k \cos(ky)\right]. \tag{44}$$

For small ϕ_k Eq. (44) gives an infinite series expansion in which the first two terms are the parallel flow $v_y = v_0 \tanh(kx)$ flow and its marginally stable eigenmode $\mathrm{sech}(kx)\cos(ky)$. For $\phi_k \to 1$ the solution represents a chain of point vortices.

From the growth of the most unstable linear eigenmode the first stage of saturation given by (44) occurs for $k = k_m = 0.377/a$, and the effective width of mean flow is likewise $a_{\text{eff}} = a/0.377 = 2.65a$ in this nonlinear state.

The simulations show that the saturated state similar to (44) is only an intermediate stage in the development of the sheared flow. In this state the counter streaming particle orbits are strongly mixing in the vortex layer and there are substantial fluctuations. The vortex chain is unstable to a fluctuation that moves two neighboring vortices closer together. The possibility of this pairing or coalescence instability is most easily seen from the point vortex limit $\phi_k \to 1$ of Eq. (44) where the analysis of Lamb[7] (p. 225) predicts instability for $q < k$ with growth rate

$$\gamma_q^{nl}(\phi_k = 1) = v_0 q(k-q)/k. \tag{45}$$

The maximum nonlinear growth rate occurs for the subharmonic mode $q = k/2$ with $\gamma_{k/2}^{nl} = kv_0/4$.

That the general distributed vortex chain is also likely to be unstable can be seen from a variational analysis of the generalized free energy[12] $F = E + C$ where $E = \frac{1}{2}\int(\nabla\phi)^2 dx\,dy$ and C is the Casimir invariant $C = \int G(\zeta)dx\,dy$ that follow from Eq. (16) $d\zeta/dt = 0$ with G chosen such that the first order variation of F, $\delta F/\delta\zeta = G'(\zeta) - \varphi = 0$, gives the equilibrium state of the system. The second order variation of F is

$$\delta^2 F = \frac{1}{2}\int\left[(\nabla\delta\phi)^2 + G''(\zeta_0)(\delta\zeta)^2\right] dx\,dy \tag{46}$$

indicates stability only when $G''(\zeta_0)$ is positive definite. For the equilibrium in Eq. (44)

the appropriate $G(\zeta)$ is

$$G(\zeta) = -\left(\frac{v_0}{2k}\right)[\zeta \ln(\zeta/kv_0) - \zeta] \tag{47}$$

for which $G''(\zeta) = -v_0^2/2\zeta(x,y) < 0$ indicating instability.

The actual growth rate $\gamma_q^{nl}(\phi_k)$ and eigenfunctions of the pairing instability are calculated numerically by Pierrehumbert and Windall.[13] They show that the nonlinear growth rate is monotonically, but weakly, increasing with $0 \leq \phi_k \leq 1$ from $\gamma_{k/2}^{nl}(\phi_k = 0) = 0.18kv_0$ to the point vortex limit $\gamma_{k/2}^{nl}(\phi_k = 1) = kv_0/4$. The stability analysis of the nonlinear state (44) by Pierrehumbert and Windall[11] indicates that the structure is most unstable to the growth of the double wavelength $q = k_m/2$ perturbation. The spanwise instability of the vortex chain in Ref. 13 is stable due to the associated magnetic field line bending $q_z v_A > \gamma_q^{nl}$ in a low β plasma.

From the nonlinear model and the tendency of like signed vortices to merge we expect the first chain of vortices with separation $2\pi/k_m$ to merge through the unstable growth of a symmetry breaking perturbation to form a chain with spacing $4\pi/k_m$, while the mean flow width $a_{\text{eff}} \to 2a_{\text{eff}}$. This process of merging may continue until the vortices reach the largest scale consistent with the geometry of the system. Now we consider the structure of the largest vortices observed in the system.

III Long-Time Stationary Vortices

At late time ($t > 10^2 a/v_0$) the flow is dominated by a few large, $R > (1-5)a$, nearly stationary vortices. From the longest simulations ($t_f \sim 10^3 a/v_0$) it appears that the long-time limit is a single large vortex with characteristic radius $R \sim L_x/2$. In this section we develop stationary vortex solutions and use them to interpret the late states of the nonlinearly saturated, quasi-stationary state.

The stationary potentials $\varphi(x,y)$ satisfying Eq. (16) are given by

$$\nabla^2 \varphi = f(\varphi). \tag{48}$$

A class of localized, analytic vortex solutions[7,14,15] are obtained by approximating $f(\varphi)$ as linear within a circle of radius r_0. For finite, localized solutions the sign of $\delta f/\delta\varphi = -\beta^2 < 0$ gives negative curvature to φ at $\pm|\varphi_{\max}|$. We introduce diagnostics to examine the validity of the relationship

$$f(\varphi) = f_0 - \beta^2 \varphi \tag{49}$$

for the observed vortices.

Defining local cylindrical coordinates about the center x_0, y_0 of the vortex

$$r(x,y) = \left[(x-x_0)^2 + (y-y_0)^2\right]^{1/2}, \qquad \cos\theta = \frac{x-x_0}{r(x,y)} \tag{50}$$

the general solution of the interior problem is

$$\varphi_i(x,y) = \varphi_0 + u_1 x + \sum_{n=0}^{\infty} G_n J_n(\beta r)\cos(n\theta) \tag{51}$$

for $r(x,y) \leq r_0$. For flows preserving the symmetry of the initial state we have $x_0 = 0, u_1 = 0$ and $G_{2n+1} = 0$.

Outside the radius r_0 the stationary vortex flow $\mathbf{v}$ is required to join continuously to the parallel flow $v_y(x)$. We make the Taylor series expansion of the parallel flow

$$v_y(x) = v_0\frac{x}{\bar{a}} - v_2\frac{x^3}{\bar{a}^3} \quad \text{for} \quad r(x,y) > r_0. \tag{52}$$

with the parameter v_2/v_0 measuring the deviation from the constant sheared flow. For the hyperbolic tangent flow $v_2 = v_0/3$. We use $a \longrightarrow \bar{a}$ in writing Eq. (52) to take into account the successive broadening of the shear layer width that occurs during the coalescence of the vortices.

We require continuity of v_r, v_θ and φ across the circle $r = r_0$ to determine the interior coefficients φ_0, G_{2n}. In the limit $v_2/v_0 = 0$ where the exterior potential becomes $\varphi_e = (v_0 r^2/4)(1+\cos 2\theta)$ the solution is given by Sagdeev et al.[14] The condition on β is

$$\beta r_0 J_2'(\beta r_0) = 2J_2(\beta r_0) \tag{53}$$

and the coefficients of the expansion (51) with $x = \beta r_0$ are

$$\begin{aligned} \varphi_0 &= \frac{v_0 r_0^2}{4\bar{a}}\left[1 - \frac{2J_0(x)}{xJ_0'(x)}\right] \\ G_0 &= \frac{v_0 r_0^2}{2\bar{a}}\frac{1}{xJ_0'(x)} \\ G_2 &= \frac{v_0 r_0^2}{4\bar{a}}\frac{1}{J_2(x)}. \end{aligned} \tag{54}$$

The first root of (53) is at $x = \beta r_0 = 6.380$ which is sufficiently into the oscillatory region of $J_0(\beta r)$ to produce a vortex with reversed flows in its outer regions $\left(\frac{r_0}{2} \leq r \leq r_0\right)$. The vortex has a tripolar structure. To eliminate the reversed flows Sagdeev et al.[14] first observe that the addition of a small term reducing the value of the coefficient 2 in (53) may

introduce a new root at smaller βr_0; they then appeal to higher order nonlinear terms of the form $\nabla^2\varphi \to \nabla^2\varphi + \frac{1}{2}(\nabla\varphi)^2$ in the Rossby wave problem to obtain a monopolar vortex solution. Here we argue that for the present problem it is the decrease of the strength of the shear in the flow occurring at finite r_0/a from the v_2 term in Eq. (52) that gives rise to the monopolar vortex. The reversed flows in the Sagdeev et al. vortex are then eliminated by the weakening of the shear in the flow at finite $r_0/\bar{a}$ by the term v_2.

For $v_2 \neq 0$ matching the exterior flow in Eq. (52) requires terms up to $G_4 J_4(\beta r)$ in expansion (51). The new dispersion relation replacing Eq. (53) is

$$\beta r_0 J_2'(\beta r_0) = 2\left[\frac{1 - \frac{v_2}{3v_0}\left(\frac{r_0}{\bar{a}}\right)^2}{1 - \frac{v_2}{6v_0}\left(\frac{r_0}{\bar{a}}\right)^2}\right] J_2(\beta r_0) \equiv \lambda J_2(\beta r_0). \tag{55}$$

The new formulas for φ_0, G_0, G_2, and G_4 are straightforward to derive. Equation (55) gives a one parameter family of vortex solutions reducing to that of Eq. (53) in the limit $r_0/\bar{a} \to 0$.

In Fig. 9 we show the vortices obtained from Eq. (53) in part a and from Eq. (55) in part b, for a typical value of $(v_2/v_0)(r_0/\bar{a})^2$. Here the separatrix is approximately elliptical in shape with $\Delta x_{sx} \simeq 0.5\bar{a}$ and length $\Delta y_{sx} \simeq 1.4\bar{a}$. The potential at the separatrix is $\varphi_{sx} = -0.10\bar{a}v_0$ and at the minimum is $\varphi_{\min} = -0.13\bar{a}v_0$.

To investigate whether the modeling of the vorticity function $f(\varphi)$ in Eq. (48) by $\delta f/\delta\varphi = -\beta^2$ is appropriate we have sampled the φ and $\nabla^2\varphi$ observed at late times in the (x, y) region of the vortex. Plots of $\zeta = \nabla^2\varphi$ versus φ from the sampling along with a least square fit to the slope are shown in Figs. 10 and 11. In Fig. 10 the vortex shown in frame (h) of Fig. 1 at $tv_0/\bar{a} = 248$ is used in the test. Here we find considerable scatter of $\nabla^2\varphi$ about $f_0 - \beta^2\varphi$ due to the incomplete coalescence of the last island pair and significant tilting. In Fig. 11 we show a case where the distortions away from an aligned, elliptical vortex are relatively small. The simulations indicate that a linear fit by $f \cong f_0 - \beta^2\varphi$ is a reasonable approximation. It is more difficult to estimate the value of βr_0 since the core radius r_0 may be considerably larger than the average radius of the separatrix as shown by the example in Fig. 9.

In the steady state there is no tilting of the vortex and thus no net momentum transport across the region outside the vortex in the dissipationless limit. Since the transport interior to the vortex separatrix is complete any collisional or stochasticity induced trapping and

de-trapping across the separatrix produces a large transport rate. The presence of a small viscosity will also lead to a finite transport rate due to a flux across the boundary layers where the ideal solutions ($\nu = 0$) have jump discontinuities in the second derivative $\partial_r^2\varphi$. In the simulations the potential $\varphi(x, y, t)$ never appears to become strictly stationary, probably due to the underlying stochasticity of the particle guiding-center motion at least in the vicinity of the separatrix flows.

IV Conclusions

There are numerous physical problems, as noted in the introduction, in which charge separation across the ambient magnetic field is established. The resulting $\mathbf{E} \times \mathbf{B}$ plasma flows may be rather arbitrary in plasmas where the collisional viscosity is weak over the space-time scales of interest. Observations and computer simulations show that plasma is able to transport momentum across the magnetic field and the natural collective electric field mechanism for this anomalous transport is through the instability driven by the gradient of the flow velocity called the Kelvin-Helmholtz instability. The self-consistent field implicit particle simulation code shows that even small flow velocity gradients produce collective oscillations that provide a strong mixing of the relative flows. The simulations show three regimes for the evolution producing the mixing of the momentum. First the quasilinear growth of the most unstable mode of the initial flow occurs terminating in a periodic chain of islands. Second the pairing and merging of the vortices occurs, and in the third stage the formation of a single, large vortex. We analyze these three regimes in this work.

In the linear regime we investigate the effect of viscosity or eddy damping on the dispersion relation finding that it reduces the cutoff wavenumber above which the principal K-H branch is stable and that it introduces new modes into the system. The viscosity coefficient may include both the collisional viscosity and that part of the small scale turbulent motions representable by a turbulent or eddy viscosity. Complete stabilization of the shear flow requires the large scale Reynolds number $R = \nu/av_0$ of order unity. The role of electron-ion dissipation is shown to provide a small threshold of the shear v_0 for instability. In addition, we consider the condition for growth and damping of the ballistic modes associated with the free streaming of an initial perturbation in the nearly collisionless plasma.

In the unstable regime, the $\mathbf{E} \times \mathbf{B}$ convection produces large scale transport of momentum through the transport flux $\pi = \langle v_x v_y \rangle$ called the Reynolds stress in the studies of neutral fluids. We calculate this transport in the quasilinear approximation and show that for a given field amplitude the momentum flux is proportional to the tilting of the axis of the vortex with respect to the direction of the parallel sheared flow. The end of the quasilinear stage of growth occurs with the tilting of the vortices going to zero and the convective flow having $\tilde{v}_x \sim \tilde{v}_y \simeq \Delta\bar{v}_y$ at scale $\lambda_x \sim \lambda_y \sim 4\pi a$. The intermediate stage starts with a long, periodic chain of vortices with $\Delta x \sim 1/k_y$ being established. The periodic vortex chain contains appreciable fluctuations due to the trapping and mixing of the particle orbits that is taking place. Because of the tendency for 2D convective nonlinearity to transfer energy to larger scales, the vortex chain is unstable to subharmonic fluctuations. Making use of a simple analytic model for the vortex chain the nonlinear stability analysis of Ref. 13 applies and gives the growth rate for the merging of the vortices. The nonlinear growth rate scales the same and is about one-half the magnitude of the linear growth rate.

In the third stage the flow fluctuates around a single, large vortex state whose scale is determined by the boundary conditions of the simulation region. We test the functional relation of the vorticity ζ and the stream function φ observed in the long time quasi-steady state finding that the relation is well described by the linear approximation $\zeta = f_0 - \beta^2\varphi$. With this linear dependence and the boundary condition that the vortex flow join to the external reversed parallel flow, we derive formulas describing the solitary sheared flow driven vortex. The formulas appear to explain the observed final state vortex.

In a dynamically adjusting sheared flow such as those that appear to occur in boundary layer plasmas such as in the edge plasma near the limiters in tokamak[11,16] confinement experiments or in the solar wind magnetosphere boundary layer.[17,18,19] We suspect that one or a number of such elliptical vortices may exist in the quiescent state with their axes parallel to the flow. Then during periods of activity where momentum is required to be transported across the shear flow boundary layer the vortex axes tilt, as for example in the quasilinear stage, to provide the required or imposed cross-field momentum transport. Pritchett and Coroniti[19] show that for $k_\perp \rho_i \lesssim 0.1$ the incompressible MHD Kelvin-Helmholtz instability agrees well with the electrostatic simulation for $v_0 \ll (c_s^2 + v_A^2)^{1/2}$ and that an ion gyroradius of order $\rho_i/a \sim 1$ is required to substantially reduce the growth rate of the fastest growing Kelvin-Helmholtz modes.

Acknowledgments

The authors thank Mr. J. Schutkeker for the computer programming presented in this work. Useful discussions with J.D. Meiss, P. Morrison, and K. Mima are also gratefully acknowledged.

This work was supported by the U.S. Department of Energy Grant no. DE-FG05080ET-53088 and the National Science Foundation Grant NSF-ATM-06646.

References

1. S. Wagner, J.R. Kan, S-I. Akasufu, T. Tajima, J.N. Leboeuf, and J.M. Dawson, in *Physics of Auroral Arc Formation,* ed. by S-I. Akasofu and J.R. Kan (American Geophysical Union, Washington, DC, 1981) p. 304.

2. J.H. Hammer and H.L. Berk, Nucl. Fusion **22**, 89 (1982); A. Reiman and R.N. Sudan, *Comments on Plasma Phys. and Cont. Fusion* **5**, 167 (1979).

3. H. L. Berk, H. Momota, T. Tajima, "Plasma Current Sustained by Fusion Particles in a Field Reversed Combination" IFSR #275 (1987).

4. D.C. Barnes, T. Kamimura, J.N. Leboeuf, T. Tajima, J. Comp. Phys. **52**, 480 (1983).

5. D. Montgomery and L. Turner, Phys. Fluids **23**, 264 (1980).

6. J. Liu, Ph.D. Dissertation, The University of Texas at Austin, 1985 and Phys. Fluids **30**, 467 (1987).

7. H. Lamb, **Hydrodynamics** (Dover, New York, 1945) pp. 212-247.

8. W. Horton, Plasma Phys. and Controlled Fusion **27**, 937 (1985).

9. S. Chandrasekhar, **Hydrodynamic and Hydromagnetic Stability** (Dover, New York, 1961) pp. 481-487.

10. M.N. Rosenbluth and A. Simon, Phys. Fluids **7**, 557 (1964).

11. T. Chiueh, P.W. Terry, P.H. Diamond, and J.E. Sedlak, Phys. Fluids **29**, 231 (1986).

12. P.J. Morrison, Bull. Am. Phys. Soc. **31**, 1609 (1986) and R.D. Hazeltine, D.D. Holm, J.E. Marsden & P.J. Morrison, in *Proceedings of the International Conference on Plasma Physics*, Eds. M.Q. Tran & M.L. Sawley (Ecole Polytechnique Federale de Lausanne, Lausanne 1984) Vol. 1, p. 203.

13. R.T. Pierrehumbert and S.E. Windall, J. Fluid Mechanics **114**, 59 (1982).

14. R.Z. Sagdeev, V.D. Shapiro, V.I. Shevchenko, Sov. Astron. Lett. **7**, 279 (1981).

15. W. Horton and J. Liu, Phys. Fluids **27**, 2067 (1984).

16. C. Ritz, R.D. Bengtson and S.J. Levinson, Phys. Fluids **27**, 2956 (1984).

17. J.G.R. Sonnerup, J. Geophys. Res. **85** 2017 (1980).

18. J.L. Burch, Rev. Space Science and Space Phys. **21**, 463 (1983).

19. P.L. Pritchett and F.V. Coroniti, J. Geophys. Res. **89**, 168 (1984).

Figure Captions

1. Evolution of the electrostatic potential for $L/a = 6.4$, $v_0/a\omega_{ci} = 0.15$, $m_i/m_e = 1600$..

2. Evolution and mixing of guiding center particles for the case in Fig. 1. Only those particles with initial negative $v_y < 0$ streaming velocity are plotted at the same times shown in Fig. 1.

3. Eigenmode frequency ω_k and growth rate γ_k for the piecewise continuous profile (2) in the limit $L_x/a \gg 1$.

4. Eigenfunction and quasilinear flux. (a) Amplitude $A_k(x)$ and phase $\theta_k(x)$ of the eigenfunction corresponding to the $m = 1$ mode. (b) Momentum flux or Reynolds shear stress $\pi(x,t)$ in the quasilinear flow.

5. Perturbed flow showing the staggered chains of convection cells produced by the eigenmode in Fig. 4.

6. Tilted vortex in the $\mathbf{E} \times \mathbf{B}$ flow produced by the sum of the perturbed flow and the equilibrium sheared flow in the quasilinear approximation.

7. Mechanism of momentum flux π due to the tilting of the vortex.

8. Effect of viscosity or eddy damping on the K-H eigenmodes.

9. The nonlinear tripolar stationary vortex of the constant shear flow ($v_2 = 0$). (b) The monopolar stationary vortex of the non-uniform sheared flow with $v_2 = v_0/3$.

10. The long-time quasi-steady vortex state (a), and (b) the functional relation of $\nabla^2\varphi = f(\varphi)$ measured in the long time, quasi-stationary vortex taken from part (h) of Fig. 1.

11. Functional relation of $\nabla^2\varphi = f(\varphi)$ taken within the core of a different vortex.

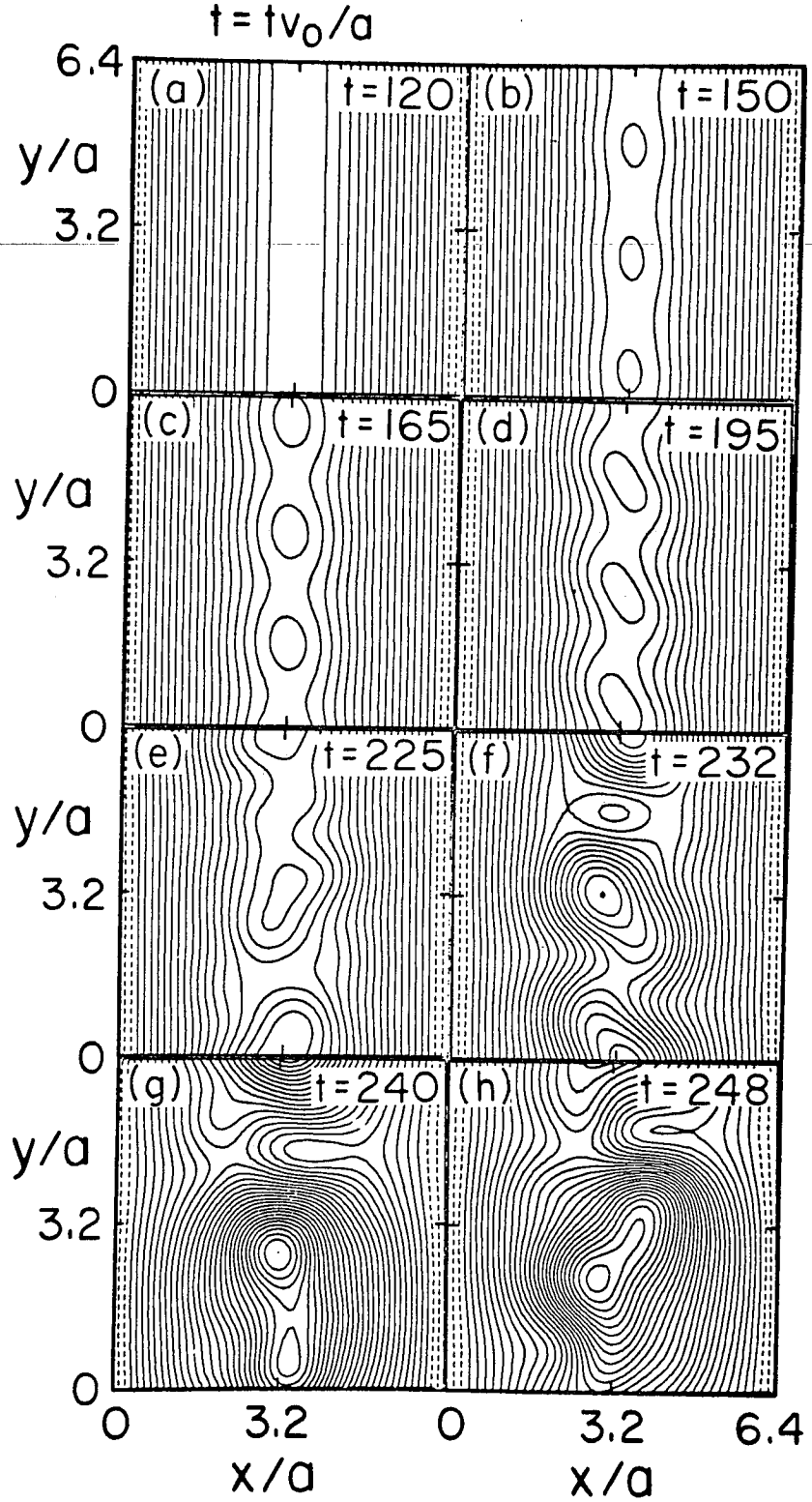
t = tv0/a
6.4
(a)
t=120
(b)
t=150
y/a
3.2
0
(c)
t=165
(d)
t=195
y/a
3.2
0
(e)
t=225
(f)
t=232
y/a
3.2
0
(g)
t=240
(h)
t=248
y/a
3.2
0
0
3.2
0
3.2
6.4
x/a
x/a

Fig. 1

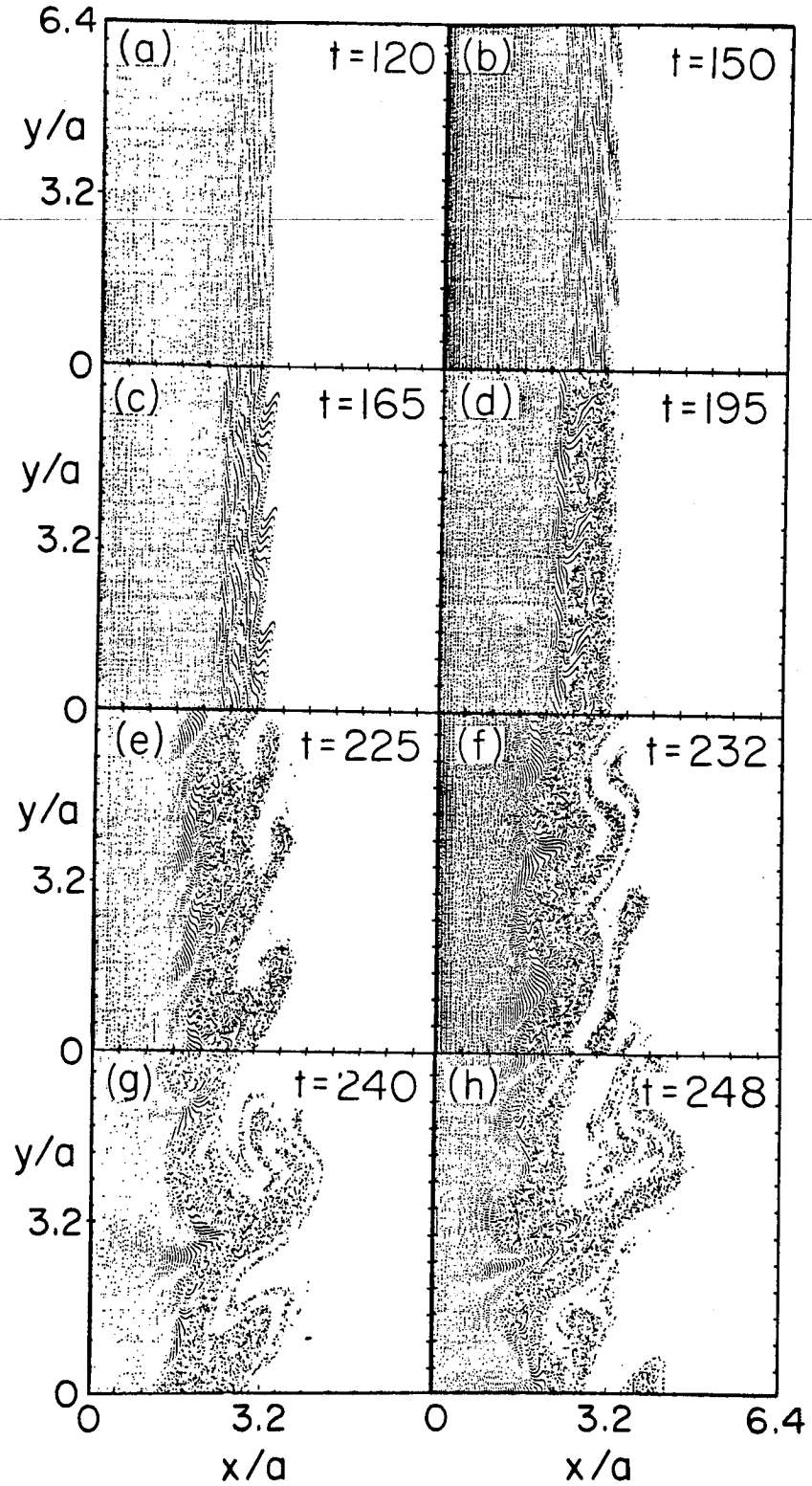
6.4
(a)
t=120
(b)
t=150
y/a
3.2
0
(c)
t=165
(d)
t=195
y/a
3.2
0
(e)
t=225
(f)
t=232
y/a
3.2
0
(g)
t=240
(h)
t=248
y/a
3.2
0
0
3.2
0
3.2
6.4
x/a
x/a

Fig. 2

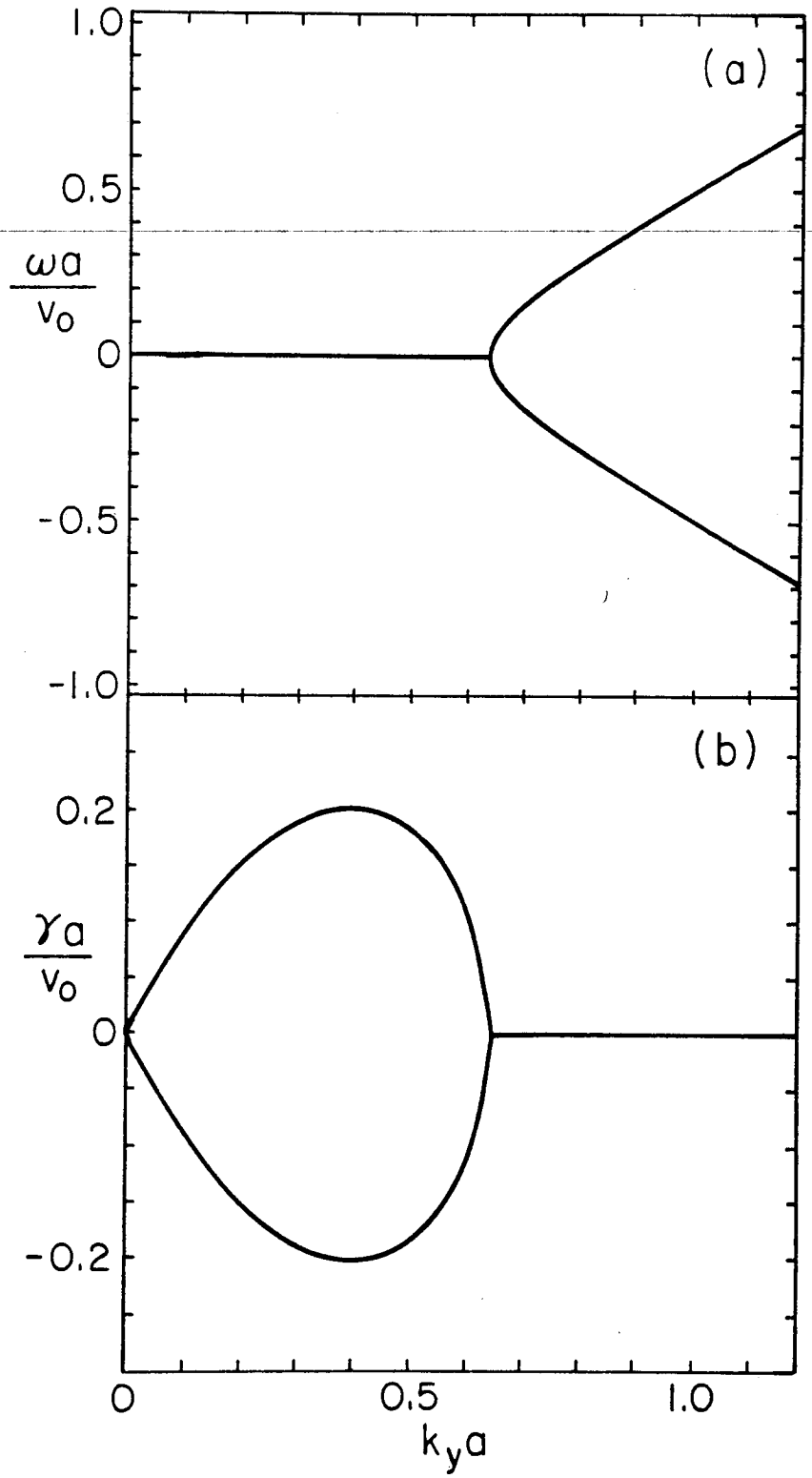

Fig. 3

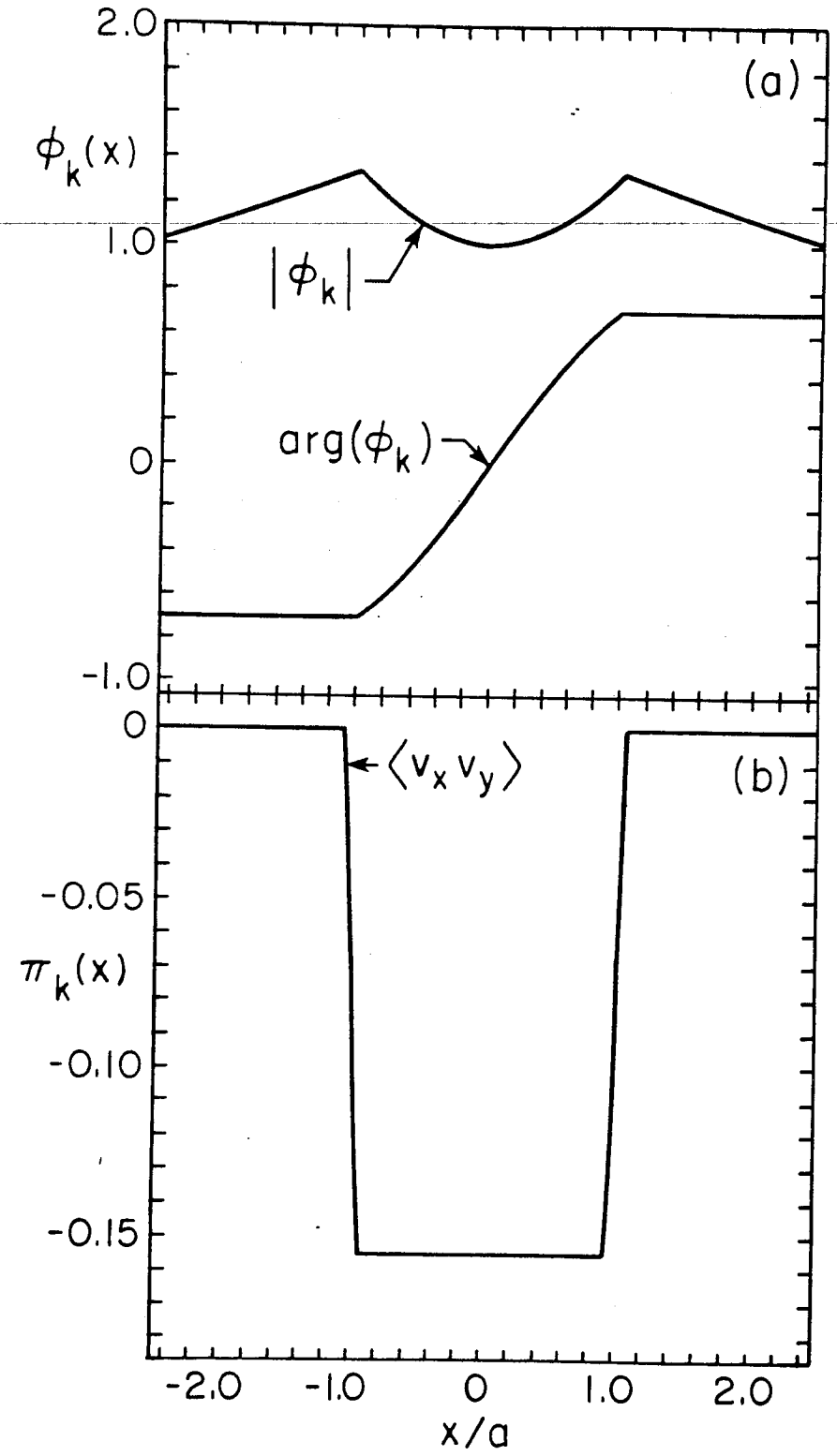
2.0
(a)
$\phi_k(x)$
1.0
$|\phi_k|$
$\arg(\phi_k)$
0
-1.0
0
$\langle v_x v_y \rangle$
(b)
-0.05
$\pi_k(x)$
-0.10
-0.15
-2.0
-1.0
0
1.0
2.0
x/a

Fig. 4

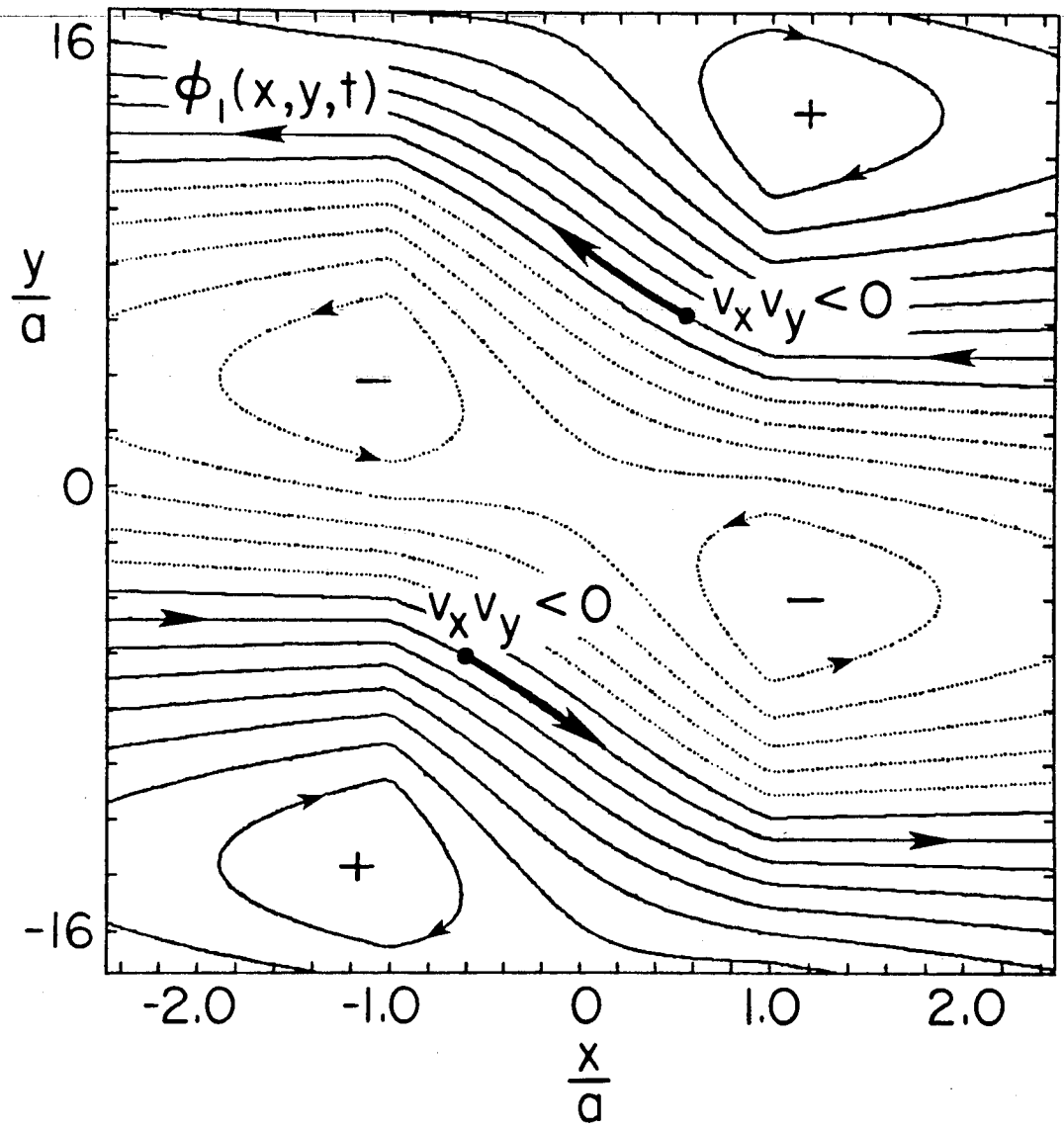

Fig. 5

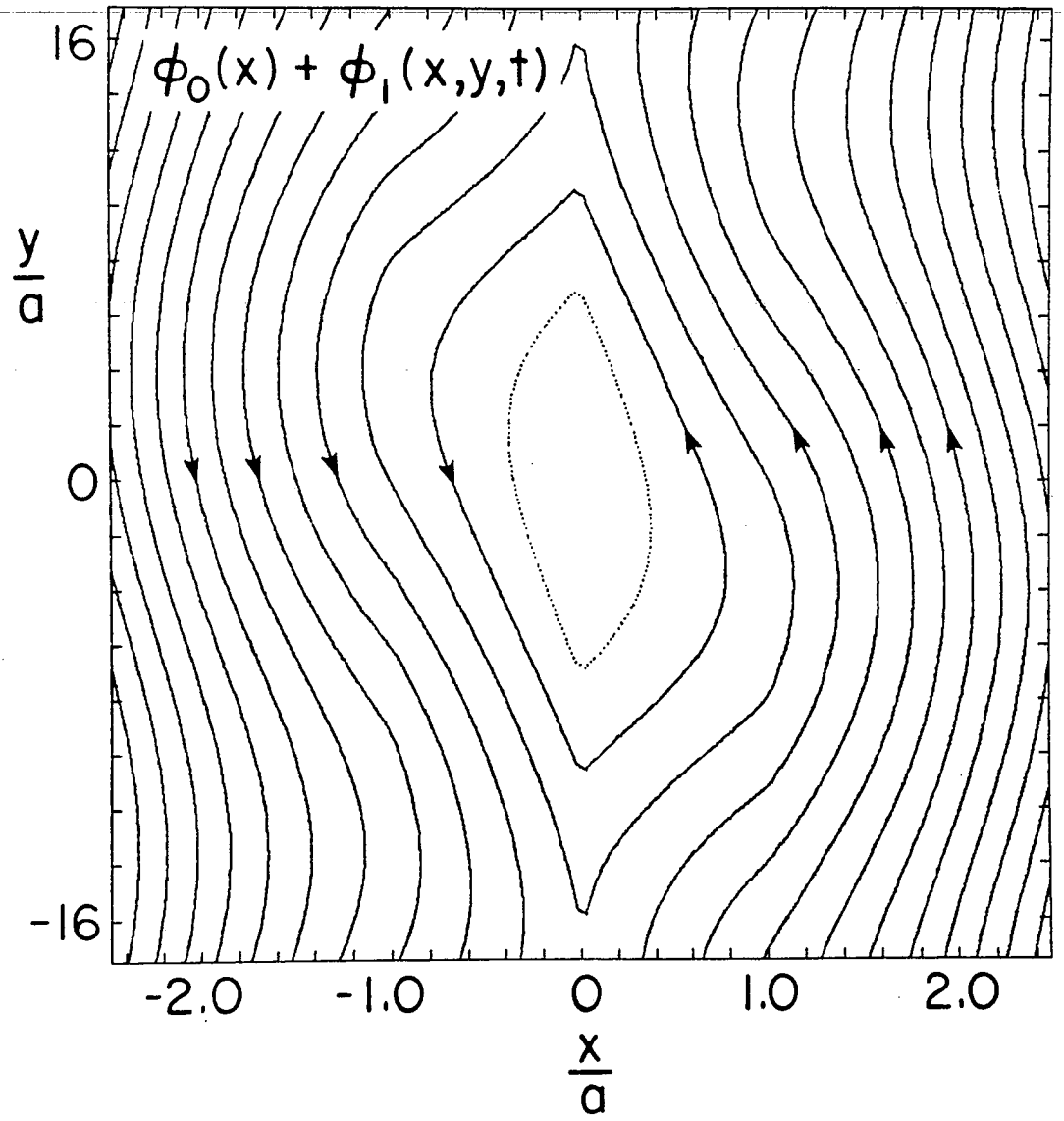

Fig. 6

K - H TILTED VORTICES

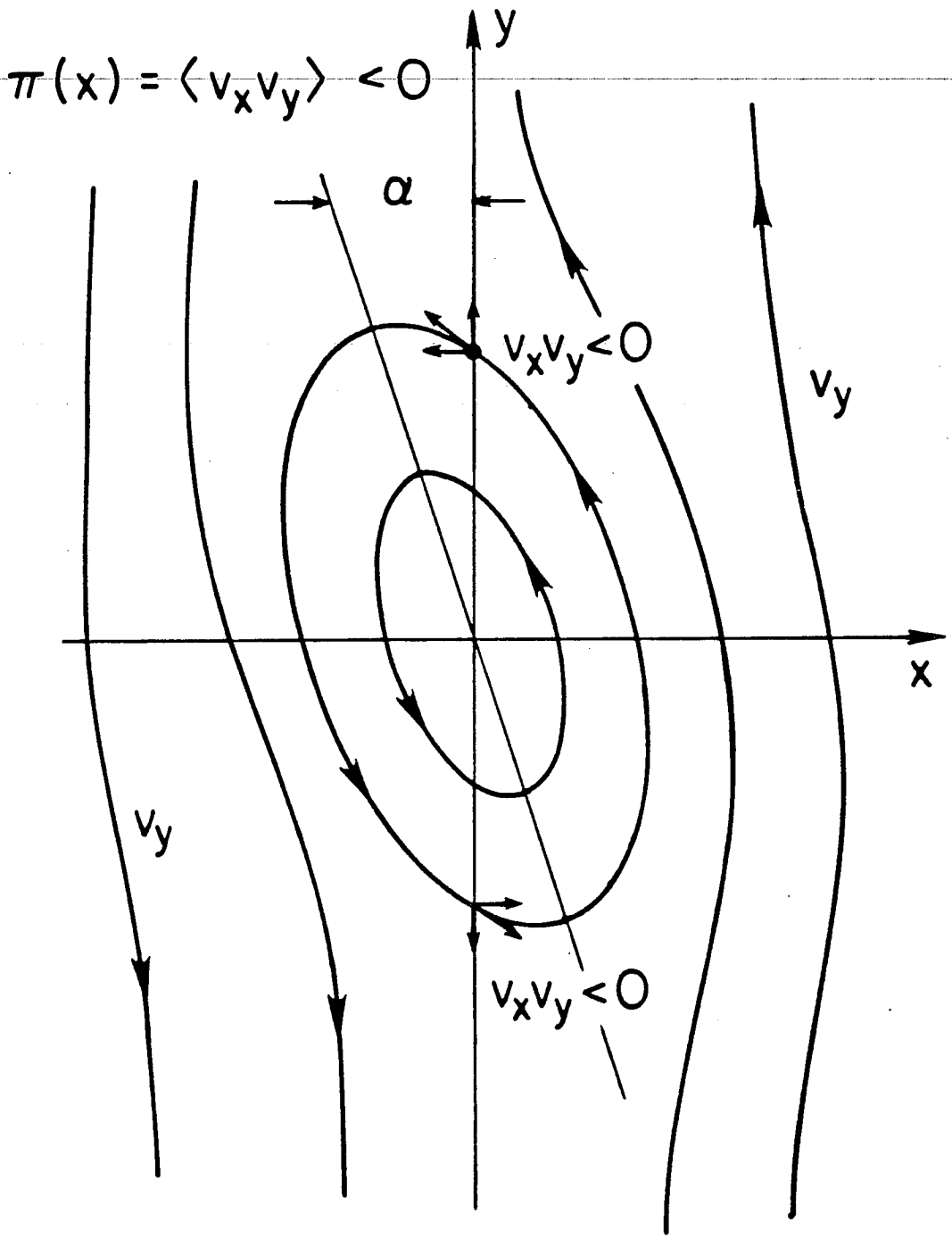

Fig. 7

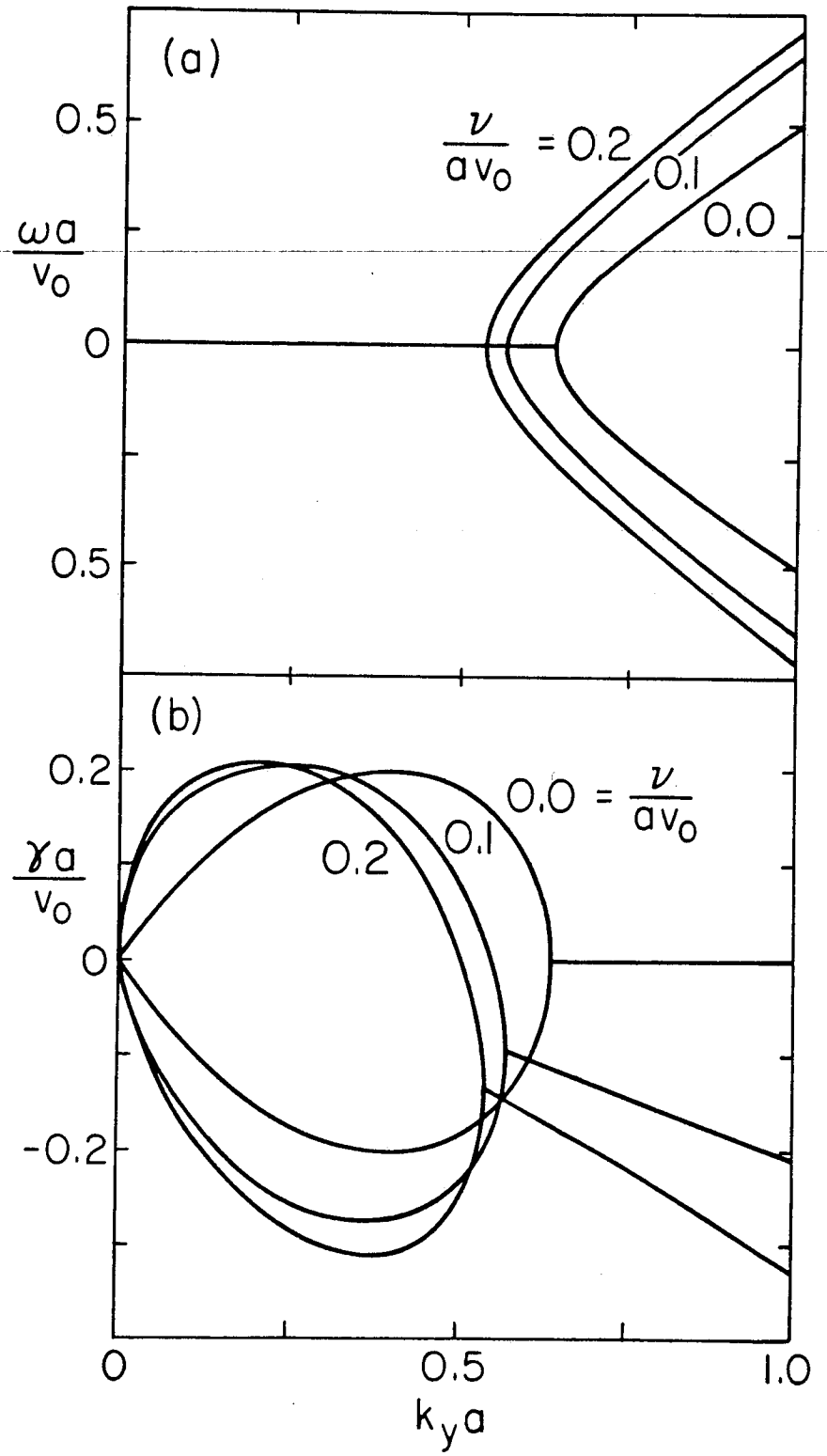
(a)
0.5
$\frac{\omega a}{v_0}$
0
0.5
$\frac{\nu}{a v_0}$ = 0.2
0.1
0.0
(b)
0.2
$\frac{\gamma a}{v_0}$
0
-0.2
0.0 = $\frac{\nu}{a v_0}$
0.1
0.2
0
0.5
1.0
$k_y a$

Fig. 8

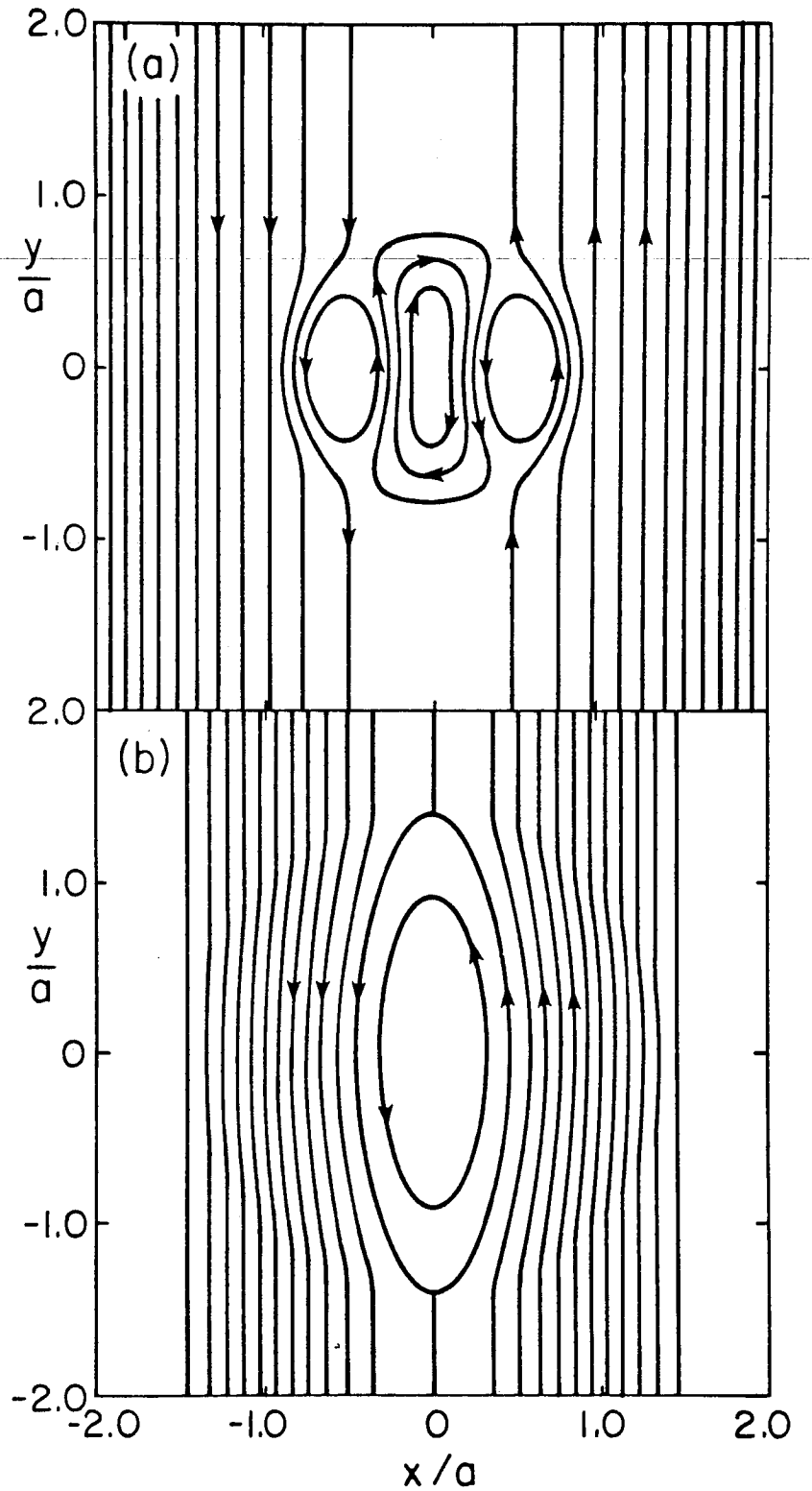

Fig. 9

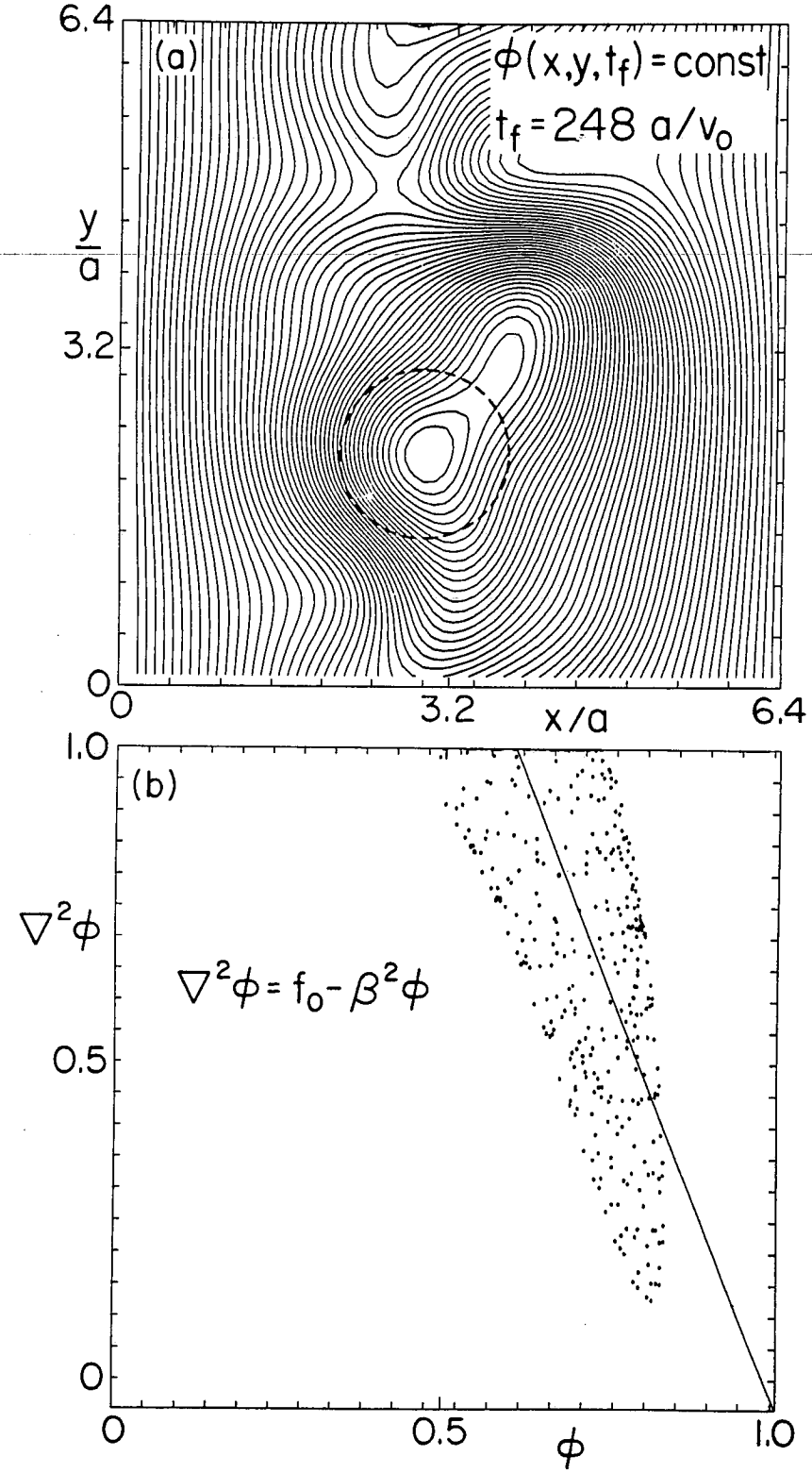
6.4
(a)
$\phi(x,y,t_f) = \text{const}$
$t_f = 248\ a/v_0$
y/a
3.2
0
0
3.2
x/a
6.4
1.0
(b)
$\nabla^2\phi$
$\nabla^2\phi = f_0 - \beta^2\phi$
0.5
0
0
0.5
ϕ
1.0

Fig. 10

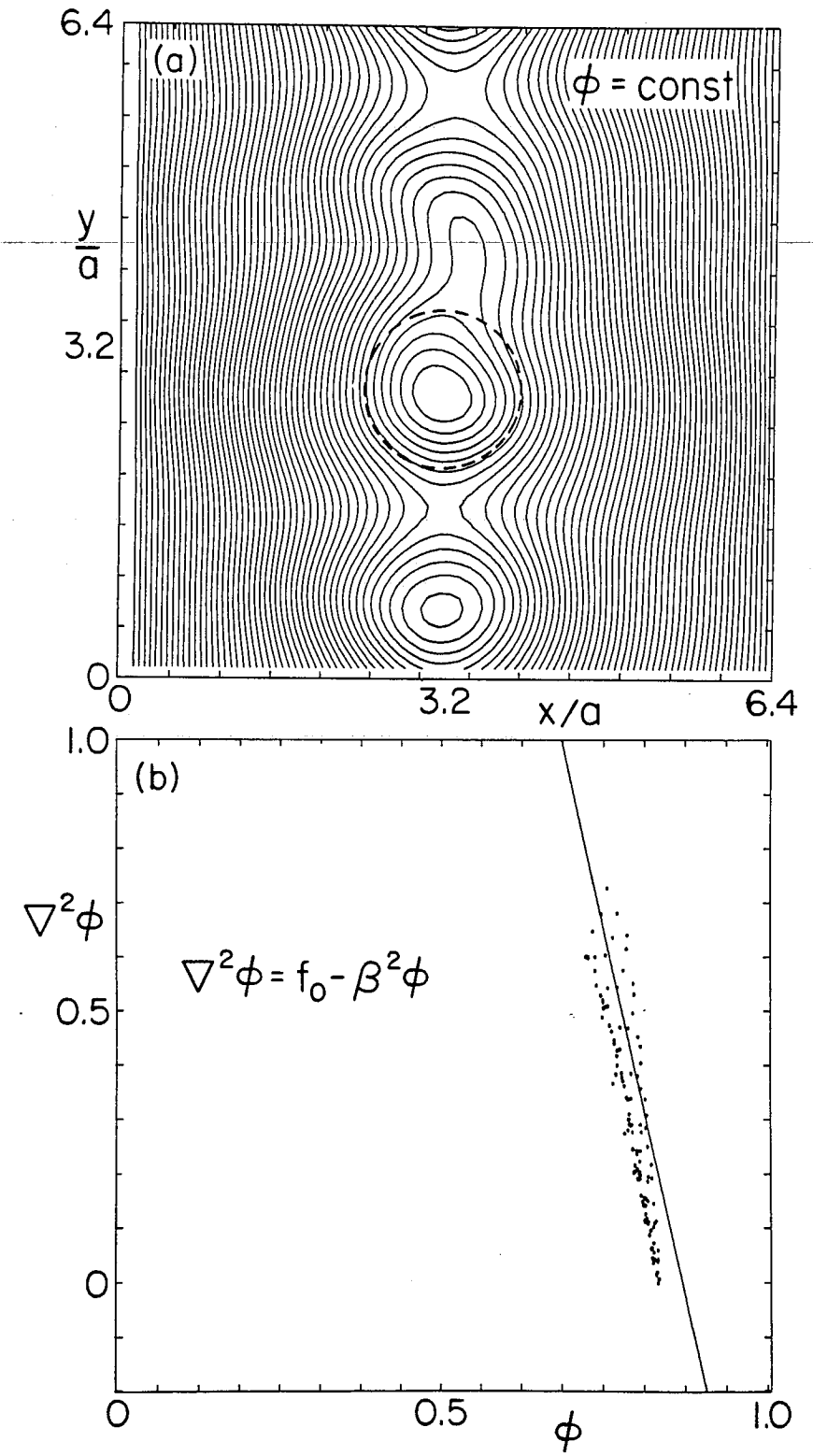
(a)
ϕ = const
6.4
y/a
3.2
0
0
3.2
x/a
6.4
(b)
$\nabla^2\phi = f_0 - \beta^2\phi$
1.0
$\nabla^2\phi$
0.5
0
0
0.5
ϕ
1.0

Fig. 11